

Supplementary Information

Functionalities of the $\text{LiV}_{3-x}\text{Nb}_x\text{O}_8$ surface layer on a Li_2NiO_2 cathode additive for enhancing the moisture stability and cycling performance of lithium-ion batteries

Jaewoo Jung,^a Yun Seong Byeon,^a Dongil Kim,^a Seong Hee Jeong,^a Chang Hoon Song,^b Eung-Ju Lee,^b Seung-Min Oh,^b Min-Sik Park^{a*}

^a Department of Advanced Materials Engineering for Information and Electronics, Integrated Education Institute for Frontier Science & Technology (BK21 Four), Kyung Hee University, 1732 Deogyong-daero, Giheung-gu, Yongin 17104, Republic of Korea

^b Battery Cell Engineering Design Team, Research & Development Division, Hyundai Motor Company, 150, Hyundaiyeonguso-ro, Namyang-eup, Hwaseong-si, Gyeonggi 18280, Republic of Korea

*Corresponding authors email address:

mspark@khu.ac.kr (M.-S. Park)

Table S1. Comparison of lattice parameters of LiV_3O_8 and $\text{LiV}_{3-x}\text{Nb}_x\text{O}_8$ ($x = 0.03$).

	a (Å)	b (Å)	c (Å)	Volume (Å ³)	α	β	γ
LiV_3O_8	6.6662	3.6070	11.8549	285.0509	90.000	104.91	90.000
$\text{LiV}_{2.97}\text{Nb}_{0.03}\text{O}_8$	6.6760	3.6081	11.8564	285.5931	90.000	104.91	90.000

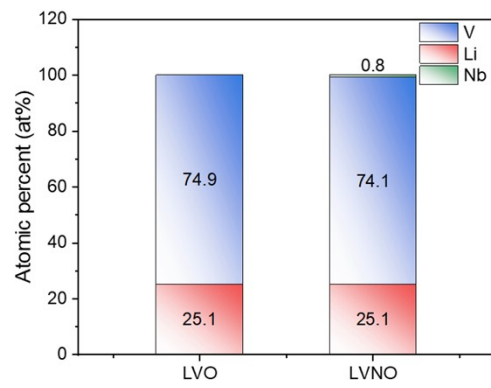


Fig. S1. ICP-MS analyses of LVO and LVNO representing compositions of Li, V, Nb.

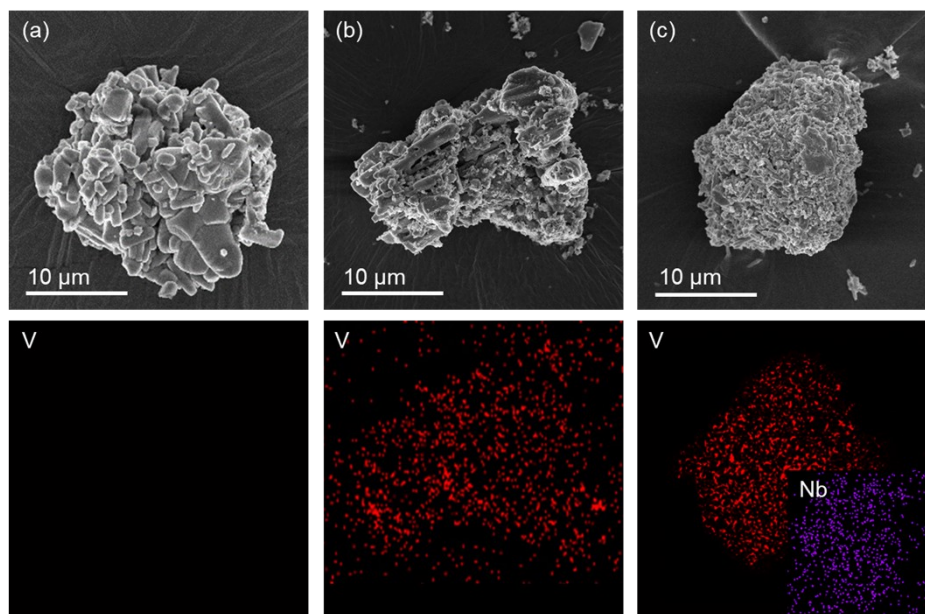


Fig. S2. FESEM images of (a) LNO (b) LVO@LNO, (c) LVNO@LNO. and corresponding EDS elemental mapping images of Li, V, Nb.

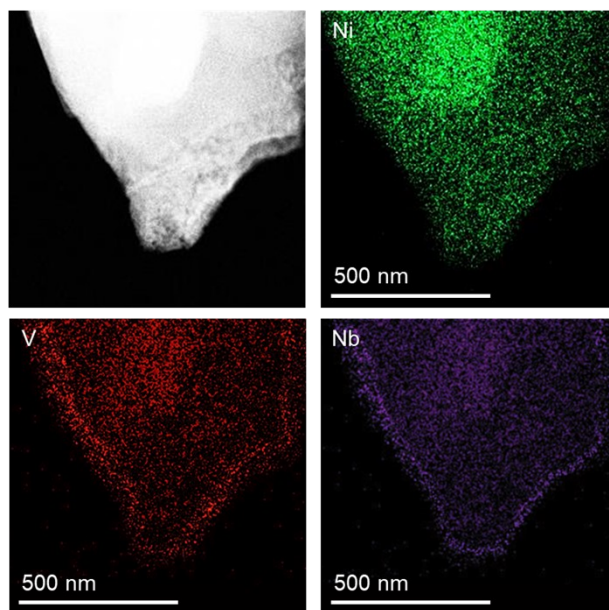


Fig. S3. A TEM image with corresponding EDS elemental mapping results of LVNO@LNO particle; Ni (green), V (red), and Nb (purple).

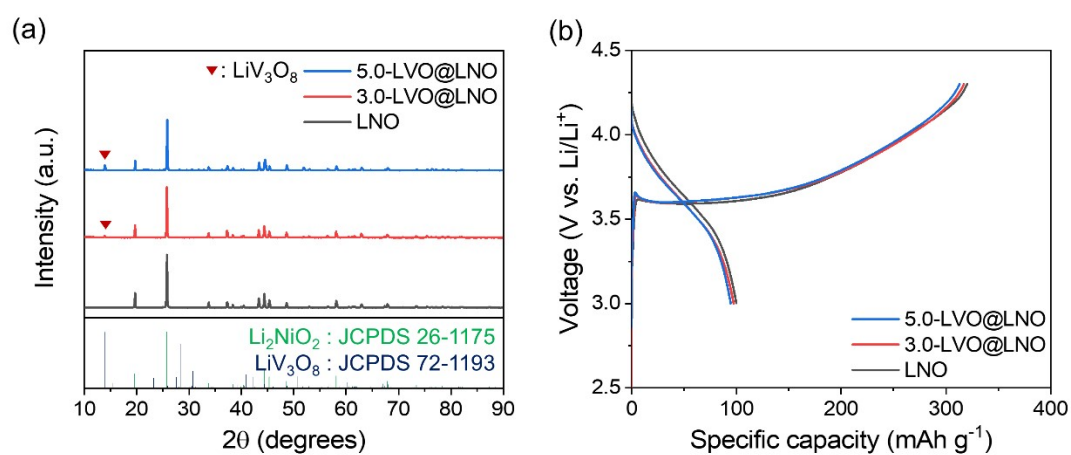


Fig. S4. (a) Powder XRD patterns of LNO, 3.0-LVO@LNO and 5.0-LVO@LNO. (b) Galvanostatic voltage profiles of LNO, 3.0-LVO@LNO and 5.0-LVO@LNO at a current density of 0.2 C ($1.0 \text{ C} = 320 \text{ mA g}^{-1}$) before air exposure.

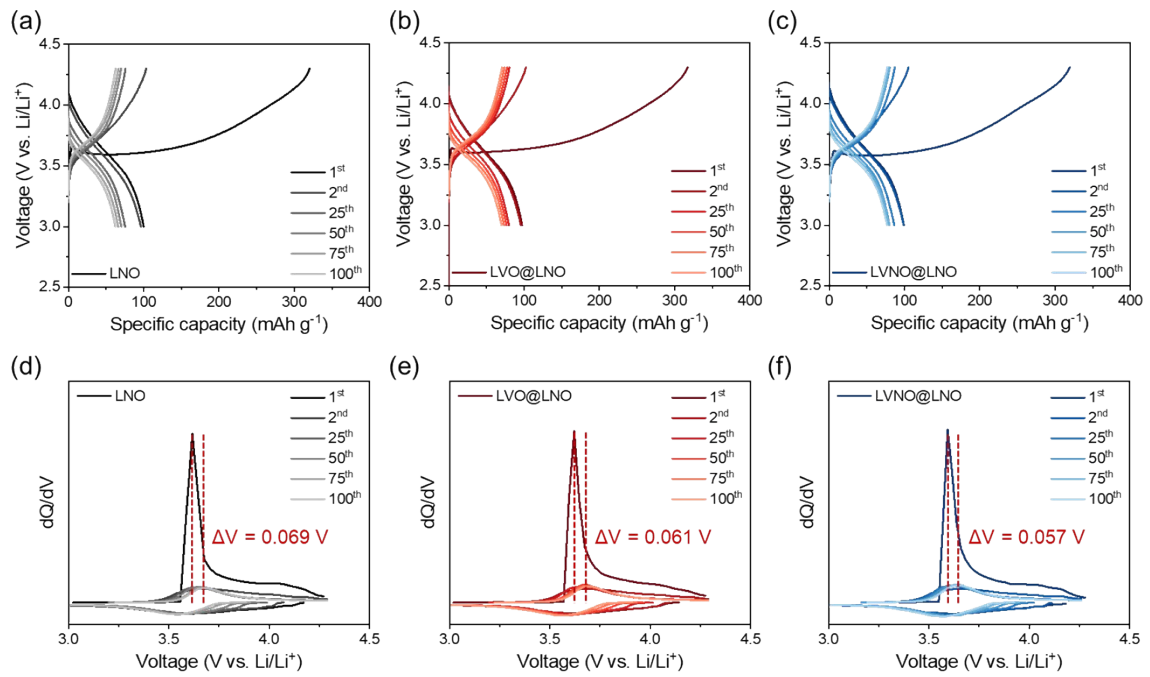


Fig. S5. Galvanostatic voltage profiles and corresponding differential voltage (dQ/dV) profiles of the (a) LNO, (b) LVO@LNO, and (c) LVNO@LNO electrodes during subsequent cycles.

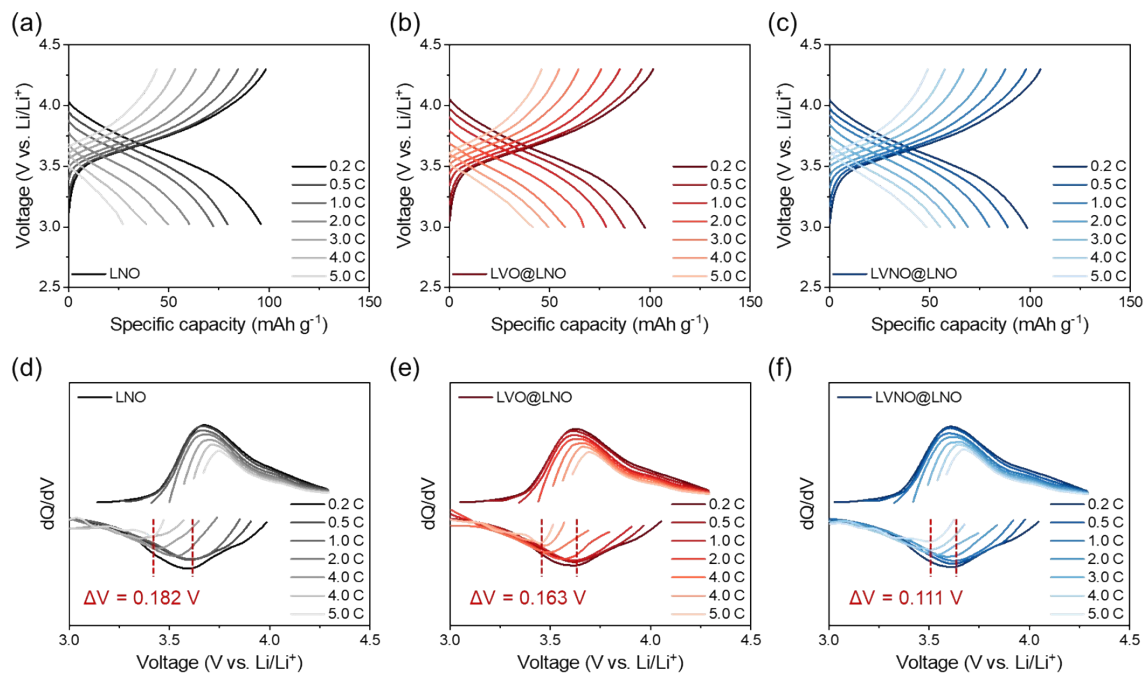


Fig. S6. Galvanostatic voltage profiles and corresponding differential voltage (dQ/dV) profiles of the (a) LNO, (b) LVO@LNO, and (c) LVNO@LNO electrodes during various current densities of 0.2–5.0 C. (1.0 C = 320 mA g⁻¹).

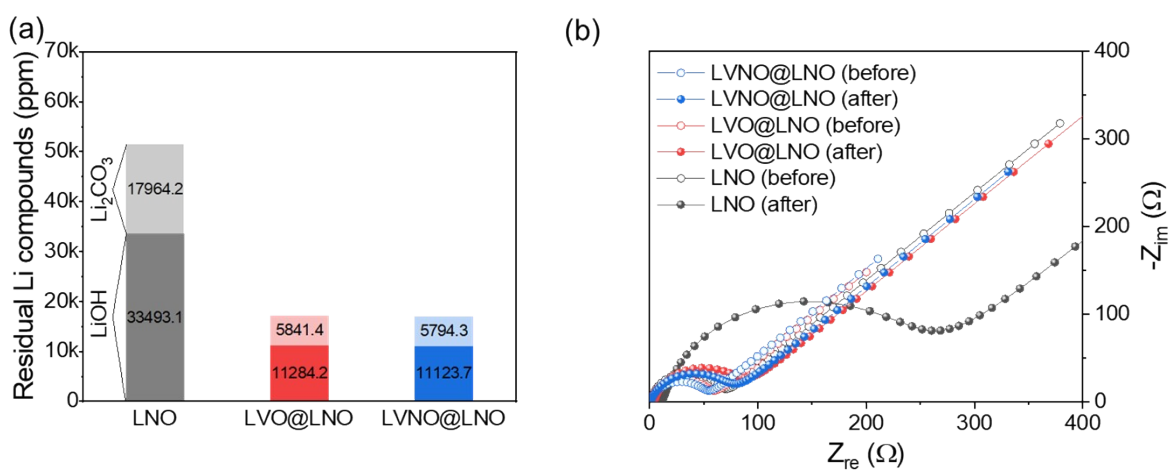


Fig. S7. (a) The potentiometric titration results for all samples after air exposure at RH 40% for 24 h. (b) Nyquist plots of before and after air exposure at RH 40% for 24 h.

Table S2. Configurations of CR2032 coin-type full-cells for electrochemical tests.

	w/o LNO	w LNO	W LVNO@LNO	graphite/SiO _x 20wt%
1 st charge capacity (mAh g ⁻¹)	238.2	246.4	246.3	599.0
1 st discharge capacity (mAh g ⁻¹)	209.7	198.7	198.6	513.3
Coulombic efficiency (%)	88.0	80.7	80.7	85.7
Loading level (mg cm ⁻²)	11.4	11.1	11.1	5.0
Electrode thickness (μm)	51.7	50.5	50.5	44.3

Table S3. Comparison of transition metal concentrations in electrolytes extracted from cells charged to 4.3 V vs. Li/Li⁺ and stored at 60°C for 48 h.

	NCM811 w/o LNO	NCM811 w/ LNO-10wt%	NCM811 w/ LVNO@LNO-10wt%
Ni (ppm)	0.017	0.014	0.009
Co (ppm)	0.007	0.006	0.002
Mn (ppm)	0.003	0.003	0.001

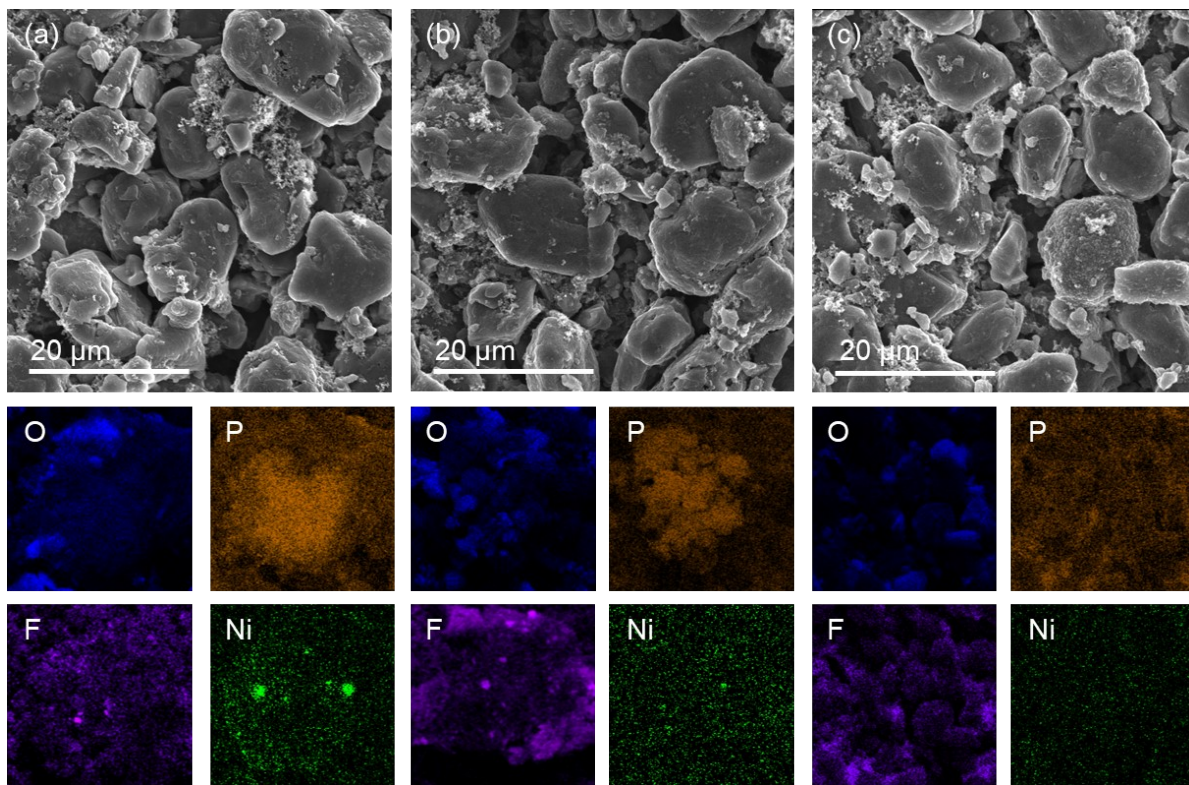


Fig. S8. FESEM images of (a) w/o LNO (b) w LNO, (c) w LVNO@LNO full-cell anodes after cycling with corresponding EDS elemental mapping results of O (blue), P (orange), F (purple) and Ni (green).